ACS OMEGA

Open Access

http://pubs.acs.org/journal/acsodf

Article

Synthesis of Kaolin-Supported Nickel Oxide Composites for the Catalytic Oxidative Degradation of Methylene Blue Dye

Kedir Seid Mohammed, Minaleshewa Atlabachew,* Belete Asefa Aragaw,* and Zinabu Gashaw Asmare

Cite This: *ACS Omega* 2024, 9, 4287−4299

Read Online

ACCESS | Metrics & More | Article Recommendations | Supporting Information

ABSTRACT: Organic dye contamination of water is a contributing factor to environmental pollution and has a negative impact on aquatic ecology. In this study, unsupported NiO and kaolin-supported NiO composites were synthesized by a one-step wet impregnation−precipitation method through the precipitation of nickel hydroxide onto locally accessible, inexpensive, and easily treated kaolin surfaces by using sodium hydroxide as a precipitating agent. The product was calcined at 500 °C and used for the catalytic oxidative degradation of methylene blue (MB) dye in an aqueous solution. The morphology, structure, and interactions of the synthesized materials were explored by SEM, XRD, and FT-IR spectroscopy. The characterization results revealed the fabrication and the growth of NiO on the kaolin surface. To determine the catalytic oxidative degradation performance of the catalyst, many experiments have been performed using the MB dye as a model dye. The catalytic degradation tests confirmed the importance of NiO and the high catalytic activity of the synthesized NiO/kaolin composite toward MB dye degradation. The oxidative degradation results showed that the optimized precursor amount on the kaolin surface could efficiently enhance the removal of MB dye. The kinetic investigation of the catalytic degradation of MB dye fitted the pseudo-first-order kinetic model. High removal efficiency was observed after eight reuse cycles, proving the exceptional stability and reusability of the composite. The catalytic process also proceeded with a low activation energy of 30.5 kJ/mol. In conclusion, the kaolin-supported NiO composite was established to be a favorable catalyst to degrade a model dye (MB) from an aqueous solution in the presence of inexpensive and easily available NaOCl with a catalytic efficiency of the material higher than 99% of the 20.3 mg catalyst within 6 min with an apparent rate constant, k_{app}, higher than 0.44625 min^{-1}, which is far better than that of the unsupported catalyst with a k_{app} of 0.0926 min^{-1} at 10 mg dose in 20 min.

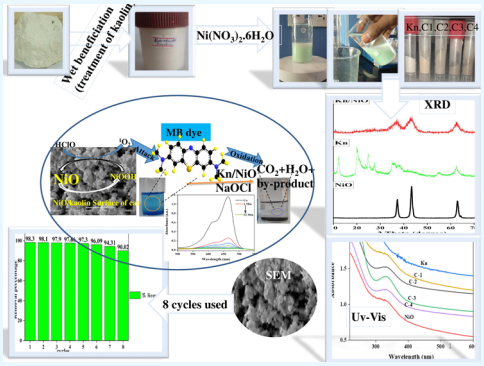

1. INTRODUCTION

All life on earth depends on water, which is a key renewable resource. For everyday human needs, forestry, raising cattle, farming, producing hydropower, industrial processes, and other applications; often known as a "unique gift of nature".[1] Contaminants such as paint, plastic, fabric, paper, leather, food, pharmaceutical, cosmetic, and other industries discharge chemicals into water bodies, which are the main source of water pollution, including dyes, chlorinated compounds, soaps, detergents, heavy metals, surfactants, salts, and inhibitory substances.[2] They are challenging to handle due to their intricate chemical composition, high solubility, and lack of biodegradability. Organic dyes are one of the main contaminants in water, particularly methylene blue dye.[3] The removal of organic dyes from water has been accomplished by a number of methods, including chemical, photochemical, coagulation, filtration, biodegradation, ultrafiltration, adsorption, and reverse osmosis.[4] However, the aromatic structural stability of these organic dyes makes their removal from water challenging, and all of the above methods have their own limitations in an application, but in the treatment of wastewater containing refractory organic materials, advanced oxidation processes (AOPs) have achieved notable advancements. They include photochemical oxidation, electrochemical oxidation, catalytic oxidation, and ozone oxidation, which have the ability to break down and transform poisonous and refractory macromolecular organic materials into safe, harmless, and biodegradable small molecular organic materials.[5]

Currently, organic pollutant catalysis is frequently carried out using metal catalysts made of Pt, Pd, Ag, and Au;[6] however, their restricted availability and rising costs limit their use. For these reasons, numerous researchers have recently become interested in easily available and inexpensive catalysts that have high catalytic efficiency and recyclability. Due to their distinctive natural characteristics, such as their restricted size,

Received: July 23, 2023
Revised: December 25, 2023
Accepted: December 29, 2023
Published: January 17, 2024

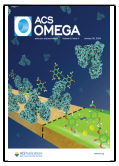

high surface-to-volume proportion, and strong catalytic activity, numerous studies have examined the properties of transition metals and their oxides as nanocatalysis[7] and has occurred as an alternative to other water treatment methods due to their effectiveness, firm process, economic feasibility, superficial usefulness of products, and no sludge production.[8] Transition metals, including cobalt, nickel, manganese, iron, copper, and their oxides, are highly employed materials for the creation of catalysts and are used to replace noble metals because of their accessibility, affordability, and chemical properties.[9]

Nickel oxide (NiO), however, has become quite popular among metal oxides. The high specific capacity, affordability, high efficiency, and accessibility of NiO nanoparticles (NPs) make them a popular choice for catalysis.[10] Numerous studies have been conducted using nickel oxide nanoparticles to photocatalytically degrade methylene blue dye.[11] However, the use of transition metals and their ions in wastewater treatment systems is limited due to their hazardous nature and difficulty in recycling,[12] and the simple ability of pure nanoparticles to aggregate prevents their usefulness and catalytic activity when utilized alone as well as the toxicity of NiO NPs and their risk to the environment and human health is still an open topic.[13] For these severe and convincing reasons, researchers have determined composites in which NPs are attached to solid matrices, restricting NP mobility without eliminating their special qualities. Numerous studies have suggested that growing nanoparticles on support materials can reduce their aggregation, which is a main concern.[14] Unfortunately, the majority of support materials are excessively costly, and the procedures involved in synthesis are difficult and time-consuming.

Clay minerals have garnered significant attention as substrates for nanoparticles because of their inherent, economic, and environmental attributes such as large surface area, superior adsorption capabilities, and capacity for ion exchange. One of the most cost-effective ways to develop nanoparticles on clay compounds is to use them as support materials. This is because clay compounds are less expensive than other support materials like carbon nanotubes and graphene, which are more expensive than inexpensive clay.[15]

Kaolin, however, has been researched for support of nanoparticles due to its affordable properties, such as accessibility, affordability, low price, abundance, and environmental approachability. It is especially necessary to act as a support for a nanocatalyst because of its exceptional features, including excellent adaptability, thermal and mechanical stability, and its layered nature makes it simple to alter and create composites and hybrids.[16] The addition of NiO NPs to the solid kaolin support facilitates retrieval of NiO NPs, promotes the adsorption of contaminants, and accelerates the catalytic degradation processes as the clay maintains NPs on its outer surfaces and in its internal voids.[17]

Additionally, the effects of using H_2O_2 as an oxidizing agent during AOPs also have limitations.[18] Therefore, it is necessary to have an optional AOP that is as good as a method using H_2O_2, but with less operational expenditure. Sodium hypochlorite with its exceptional oxidation capacity in neutral, acidic, and less basic solutions is frequently used in water treatment[19] for the removal of organic and inorganic substances[20] and disinfection.[21] Sodium hypochlorite has the ability to decay quickly in the presence of metal ion catalysts, and nickel-like catalysts offer the benefits of uniform dispersion, low cost, and high catalytic activity.[22]

Therefore, in this work, NiO/kaolin nanocomposite was synthesized using inexpensive, easily available kaolin and relatively low-cost chemicals like nickel nitrate hexahydrate through a simple solution-based method. The catalytic oxidation activity of the NiO/kaolin nanocomposite was used to degrade a model MB dye by using NaOCl as an oxidizing agent. The synthesized heterogeneous catalyst showed excellent catalytic activity.

It has been reported that the use of Ethiopian kaolin as an efficient support material for silver nanoparticles for the conversion of toxic MB dye to the less-toxic leuko-methylene blue byproduct using $NaBH_4$ as a reducing agent.[23,24] However, in this work, we introduced an oxidation-based degradation of MB dye to other less-toxic byproducts (CO_2, H_2O, and low-molecular-weight organics) using inexpensive and a less-toxic oxidizing agent NaOCl, and an extremely inexpensive precursor material ($Ni(NO_3)_2{\cdot}6H_2O$).

2. MATERIALS AND METHODS

2.1. Materials. Kaolin stone, nickel nitrate hexahydrate ($Ni(NO_3)_2{\cdot}6H_2O$, 99.99%, Samir Tech-Chem Pvt, Ltd.), sodium hypochlorite (NaOCl, 4%, Savgan Heights plc), methylene blue dye (MB, $C_{16}H_{18}ClNS$, Dallul Pharmaceuticals plc), and sodium hydroxide (NaOH, 98% Unichem Chemicals) were used without additional purification, and deionized water was used for all solution preparation.

2.2. Methods. *2.2.1. Treatment of Raw Kaolin Clay.* The clay that was used as a support for NiO NPs was imported to the laboratory, and its treatment was performed based on the method reported by Asmare et al.[24] with slight modifications. A certain amount of raw kaolin clay was ground with mortar and pestle and passed through a 200 mm sieve. It was soaked and stirred in distilled water for 24 h to dissolve any undesirable soluble content. It was then washed with deionized water and allowed to dry in air to obtain clay paste. The paste was then dried overnight in an oven at 70 °C. Finally, the material was crushed, sieved, and stored for analysis.

2.2.2. Synthesis of Unsupported Nickel Oxide Nanoparticles (NiO NPs). The synthesis of unsupported NiO NPs was achieved by the co-precipitation method developed by Zhang et al.[25] with slight modifications. Nickel nitrate hexahydrate ($Ni(NO_3)_2{\cdot}6H_2O$) and sodium hydroxide (NaOH) were used to create NiO NPs, and the solutions were mixed dropwise in a 150 mL beaker. The solutions consisted of 50 mL of 0.034 M $Ni(NO_3)_2{\cdot}6H_2O$ and 0.3 M NaOH. NaOH was added dropwise to the mixture until a pH of 12 was reached. A green nickel hydroxide precipitate was produced after the entire liquid had been magnetically agitated for 2 h. The filtrate was removed from the resulting precipitate and washed three times with deionized water. Additionally, the green precipitate of nickel hydroxide ($Ni(OH)_2$) was dried in an oven at 70 °C for several hours before being calcined at 500 °C for 3 h in order to obtain NiO NPs.

2.2.3. Synthesis of the Kaolin-Supported Nickel Oxide (NiO/kaolin) Nanocomposite. A wet impregnation method was used to prepare the nickel-based catalyst through a modification of the method developed by Moumen et al.[26] 1 g of treated kaolin clay was spread in 50 mL of distilled water and mixed for about 35 min. To this solution was added 50 mL of nickel nitrate hexahydrate solution (0.02M) and the mixture was agitated for an hour. Then, sodium hydroxide (0.3 M) was

https://doi.org/10.1021/acsomega.3c05126
ACS Omega 2024, 9, 4287−4299

Scheme 1. Wet Impregnation of NiO NPs Supported on the Kaolin Pores by Soaking in $Ni(NO_3)_2{\cdot}6H_2O$ Solution and Precipitating Using NaOH as a Precipitating Agent and Calcined at 500 °C

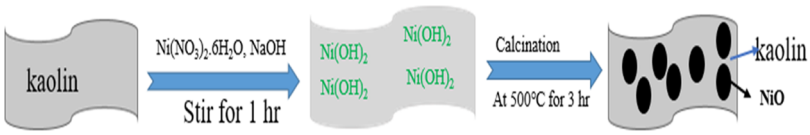

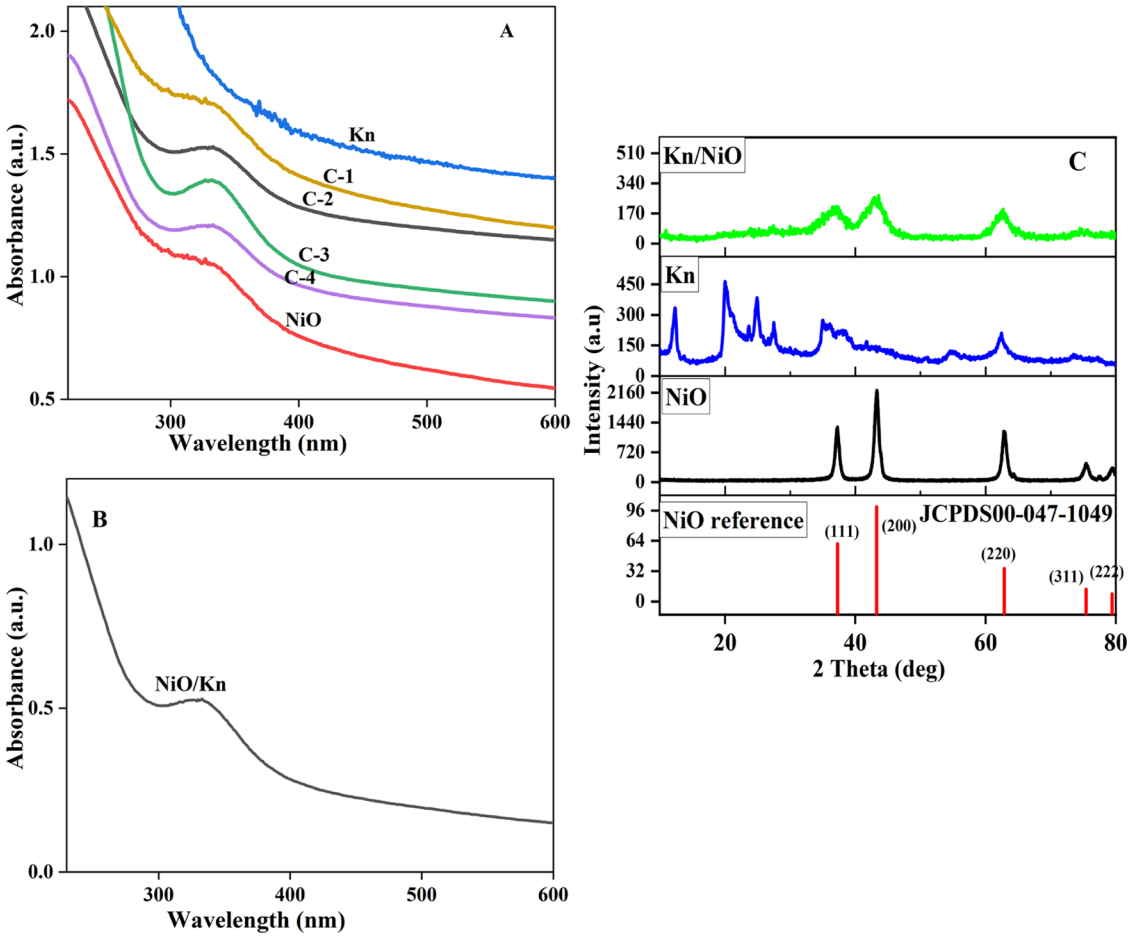

Figure 1. UV−vis spectra of (A) kaolin (Kn), NiO/kaolin nanocomposite-1 (C-1), NiO/kaolin nanocomposite-2 (C-2), NiO/kaolin nanocomposite-3 (C-3), NiO/kaolin nanocomposite-4 (C-4), and NiO NPs without the support and (B) after two months. (C) XRD spectra of NiO/kaolin nanocomposite-2 (Kn/NiO), kaolin (Kn), and unsupported NiO NPs.

added to the suspension until a pH of 12 was reached, and the mixture was stirred for 1 h. The solid catalyst product was separated by filtration and then washed with deionized water three times to remove the nickel ion residue. The obtained residue was dried in an oven at 70 °C overnight and calcined at 500 °C for 3 h and stored as NiO/kaolin nanocomposite-1. These procedures were repeated three times, with the same path for comparison, by using 0.027, 0.034, and 0.041 M $Ni(NO_3)_2{\cdot}6H_2O$, and in total four composites were prepared with different mass compositions of the nickel nitrate hexahydrate precursor. The four catalysts were named as NiO/kaolin nanocomposite-1, NiO/kaolin nanocomposite-2, NiO/kaolin nanocomposite-3, and NiO/kaolin nanocomposite-4. Scheme 1 shows the synthesis mechanism of the NiO/kaolin nanocomposite using NaOH as a precipitating agent.

2.3. Characterization Techniques. An XRD-7000 X-ray diffractometer (Shimadzu, Japan) was used to obtain X-ray diffraction (XRD) patterns of the support kaolin and NiO/kaolin nanocomposite. A UV−vis spectrophotometer (HACH DR6000, Linderberg Drive, Loveland) was used to obtain the absorption spectra. An FT/IR-6600, FTIR spectrometer (JASCO International Co., Ltd., Tokyo, Japan) was used to record Fourier transform infrared (FT-IR) spectra between 4000 and 400 cm^{-1}. A JEOL NeoScope JCM-6000Plus Benchtop SEM (HITACHI, Japan) was used to obtain scanning electron microscopy (SEM) images.

2.4. Catalytic Activity of NiO/Kaolin Nanocomposites on MB Dye. In the present work, a NiO/kaolin nanocomposite was used as a catalyst to degrade MB dye by using NaOCl as an oxidizing agent. A mass of 10 mg of the NiO/kaolin nanocomposite was mixed with 50 mL of 50 ppm MB in the presence of 4% NaOCl (0.5 mL). The kinetics of the catalytic oxidation of MB using the NiO/kaolin nanocomposite was examined using UV−vis spectroscopy by tracking the highest absorption wavelength of MB until it completely disappeared (λ_{max} = 664 nm). The dark blue color

https://doi.org/10.1021/acsomega.3c05126
ACS Omega 2024, 9, 4287−4299

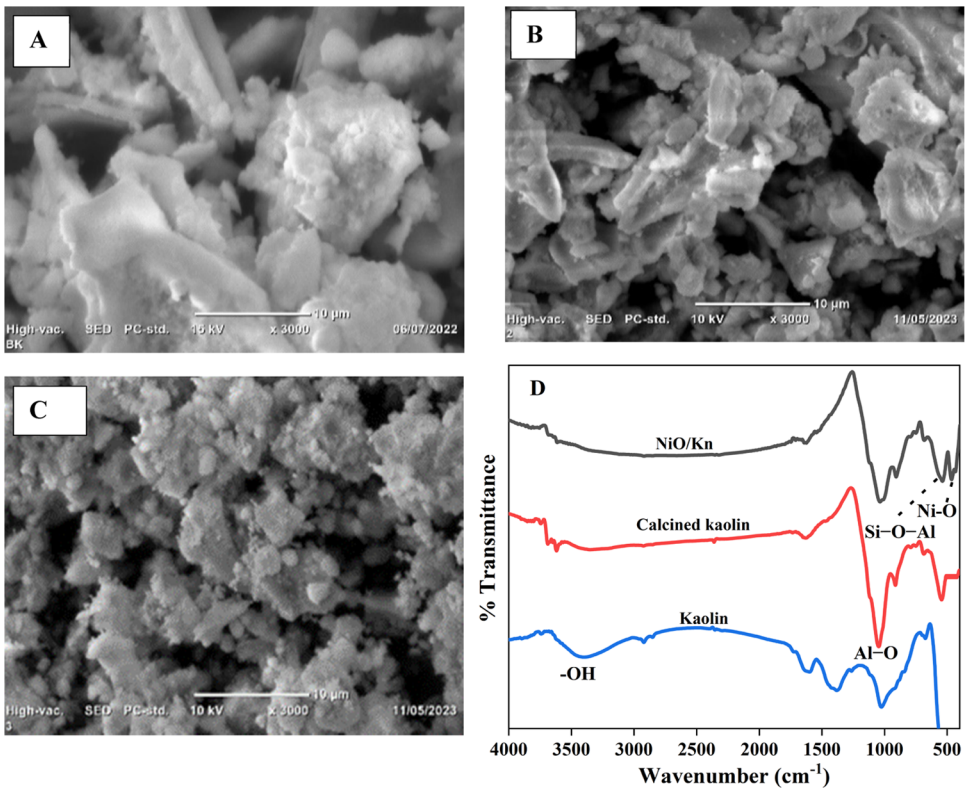

Figure 2. SEM micrographs of (A) kaolin, (B) calcined kaolin, and (C) NiO/kaolin. (D) FT-IR spectra of kaolin, calcined kaolin, and the prepared nanocomposite.

of the MB dye solution quickly disappeared. The concentration of the MB dye solution was determined by measuring the time-dependent absorbance at 664 nm using a UV−vis spectrometer (200−800 nm range). The major influences on the oxidation rate constants, including the temperature, concentration of the MB dye solution, and mass of the NiO/kaolin nanocomposite were also examined. Additionally, the effects of the NiO amount on the catalytic removal of kaolin were investigated by the oxidative removal of MB using kaolin, NiO/kaolin nanocomposite-1, NiO/kaolin nanocomposite-2, NiO/kaolin nanocomposite-3, and NiO/kaolin nanocomposite-4. The rate of oxidative degradation of the MB dye, k_{app}, is calculated using pseudo-first-order kinetics according to eq 1[23]

$$\ln\left(\frac{C_t}{C_o}\right) = -k_{app}t \tag{1}$$

where k_{app} is the degradation rate constant, C_t is the MB dye concentration at time t, and C_o is the starting MB dye concentration. The percentage degradation efficiency, D, of the catalyst was also calculated by eq 2[23]

$$\%D = \frac{C_o - C_t}{C_o} \times 100 \tag{2}$$

where C_o is the initial MB dye concentration (mg/L) and C_t is an equilibrium MB dye concentration (mg/L).

2.5. Reusability Test. To assess the reusability of the NiO/kaolin nanocomposite, its sequential catalytic activities were investigated. In the first cycle, 0.5 mL of 4% NaOCl and 25 mL of MB dye solution (100 mg/L) were combined with 10 mg of the NiO/kaolin nanocomposite. After 15 min of stirring, the mixture was screened by centrifugation at 3500 rpm for 5 min, and the NiO/kaolin nanocomposite was recycled eight more times under the same conditions, dried, and characterized by XRD to evaluate its change after eight reuse cycles.

3. RESULTS AND DISCUSSION

3.1. Characterization of NiO and the NiO/Kaolin Nanocomposite. *3.1.1. Ultraviolet−Visible (UV−vis) Spectroscopy Analysis.* For the purpose of characterizing the metal and metal oxide nanoparticles, the nanoparticle solution displays an absorption band and provides details on their size, shape, stability, and aggregation in the wavelength range of 200−800 nm.[27] NiO NPs display a distinct absorbance peak between 300 and 350 nm.[28] The UV−vis spectra of the as-synthesized NiO/kaolin nanocomposites with various precursor quantities and treated kaolin are shown in Figure 1A. The ranges showed a distinctive absorbance peak at around 333 nm, confirming the creation of NiO NPs on kaolin, as shown in Figure 1A. Furthermore, no noticeable changes in the peak location or intensity were noticed after the sample was kept in the lab for up to two months, indicating the high stability of the created kaolin-supported NiO nanocomposites, as shown in Figure 1B.

3.1.2. X-ray Diffraction Analysis. The structures of kaolin, kaolin-supported NiO nanocomposite, and NiO NPs alone were also examined by X-ray diffraction spectroscopy. The spectra showed noticeable diffraction patterns and Miller indices at 37.22° (111), 43.28° (200), 62.89° (220), 75.45° (311), and 79.46° (222), in agreement with the reference card number JCPDS00-047-1049, revealing the formation of crystalline NiO NPs (Figure 1C).[29] The absence of noticeable impurity peaks indicated that a pure NiO nanoparticle is

https://doi.org/10.1021/acsomega.3c05126
ACS Omega 2024, 9, 4287−4299

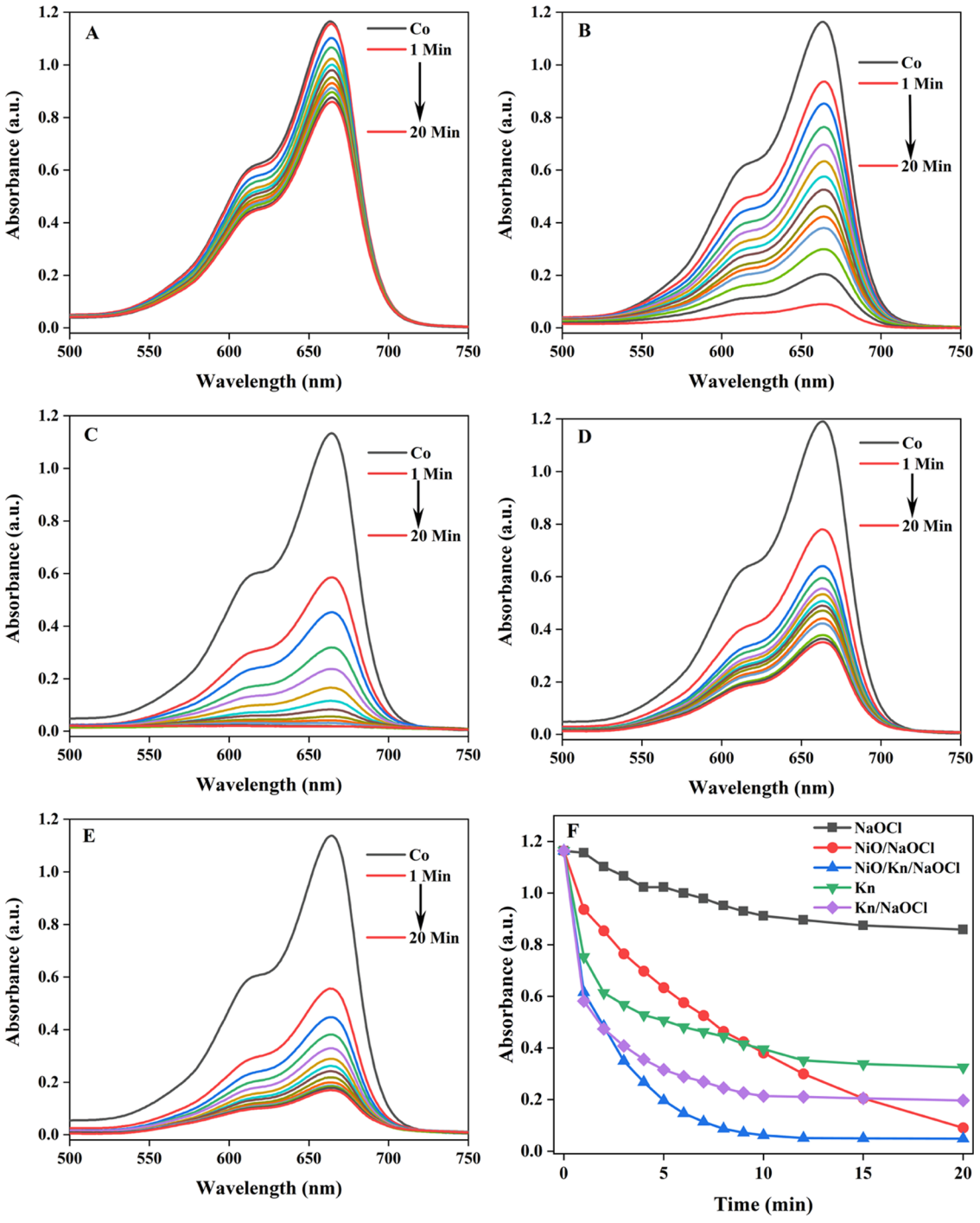

Figure 3. Removal of MB dye with different materials: (A) NaOCl, (B) NiO/NaOCl, (C) NiO/kaolin/NaOCl, (D) kaolin, (E) kaolin/NaOCl, and (F) degradation profile. Conditions: 10 mg of kaolin, NiO, NiO/kaolin; 50 mL (50 mg/L) of MB dye; 0.5 mL of NaOCl; 40 °C temperature.

formed. Additionally, the results of the literature reports on NiO NPs are consistent with our results.[30] By application of the Debye−Scherrer formula, the mean crystallite size of unsupported NiO NPs was determined to be 11 nm. The XRD patterns of the NiO/kaolin nanocomposite also showed diffraction peaks at 2θ = 37.02, 43.07, 62.52, 75.59, and 79.33°, which were assigned to NiO,[31] with various hkl values (111), (200), (220), (311), and (222), respectively, showing the decoration of kaolin by face-centered cubic (fcc) NiO NPs with an estimated average crystalline size of 3 nm (Figure S-1). The structure of kaolin is transformed from the crystalline structure to the amorphous metakaolin phase during calcination at 500 °C while making the NiO crystal. The diffraction peaks at around 2θ of 20.3 and 24.4° in Figure S-1 indicate the diffraction pattern of kaolinite in the NiO/kaolin nanocomposite.[32] In addition, the surface coverage of kaolin by NiO prevents the X-ray from accessing the kaolinite structure, and the intensity of diffraction peaks may be weak. Therefore, the semi-amorphous structure of kaolinite is maintained.

3.1.3. Scanning Electron Microscopic Analysis. SEM reveals the microstructure of the coated surface of the nanoparticles, catalyst distribution over the substrate surface,

https://doi.org/10.1021/acsomega.3c05126
ACS Omega 2024, 9, 4287−4299

homogeneity and heterogeneity, and also the morphology of the particles. The morphological properties of calcined kaolin, the NiO/kaolin nanocomposite, and beneficiated kaolin were examined using SEM. When compared to beneficiated and calcined kaolin, Figure 2 illustrates how the surface morphology and roughness of kaolin are altered by the addition of NiO NPs. This confirms the effective deposition of NiO NPs on the kaolin surface. The physicochemical properties of the studied kaolinite have already been reported.[23] The EDS analysis of the reported work indicates that the Ethiopian kaolinite has Si/Al of 28.01/12.33 (by mass percent) and 20.19/9.25 (by atomic percent).[23,33]

3.1.4. Fourier Transform–IR Spectroscopy Analysis. The FT-IR spectra of kaolin, calcined kaolin, and the NiO/kaolin nanocomposites are presented in Figure 2D. The main peaks appearing in the infrared region reflect Al–O, Al–OH, and Si–O functional groups in the low-frequency bending modes and high-frequency stretching.[34] The band at around 1620 cm^{-1} is related to the vibration of the water molecules. The peaks at around 1082 and 1380 cm^{-1} are related to Al–O and silicon monoxide (Si–O) stretching vibrations, which correspond to quartz and disilicon oxide (Si–O–Si) symmetric stretching vibrations, respectively, showing that silicon oxide is confined predominantly in kaolin.[33] The small peak at around 2359 cm^{-1} is ascribed to the bending of hydroxyl from the water molecule. The small peak at around 780 cm^{-1} is believed to be caused by metal impurities bound to aluminum and hydroxyl (Al-MgOH) vibrations. A peak at 530 cm^{-1} is related to Si–O–Al bending, indicating that aluminum oxide is also enclosed close to silicon oxide and the asymmetric Si–O–Si stretching vibrations were observed at about 1039 cm^{-1}. The absorption band at 465 can be assigned to the stretching vibration of the Ni–O bond, indicating the presence of NiO particles.[26,34] The broadband peak of kaolin at around 3420 cm^{-1} characterizes –OH stretching vibrations (Al–OH or Si–OH) and the band of kaolin and it was lost during calcination in calcined kaolin and composite because calcination causes structural transformation of kaolin, including sintering, dehydroxylation, and the formation of gehlenite, anorthite, and mullite.[35]

3.2. Catalytic Oxidative Activity Test. *3.2.1. Catalytic Oxidative Degradation of MB Dye.* By employing NaOCl as an oxidizing agent for MB dye oxidative degradation, we investigated the catalytic oxidative degradation reaction of the NiO/kaolin nanocomposite. A solution containing MB exhibits a UV–vis spectrum with peaks at 290 and 664 nm, accompanied by a dip at 612 nm, associated with $\pi \rightarrow \pi^*$ and $n \rightarrow \pi^*$ transitions, consequently.[36]

3.2.2. Catalytic Activity of the NiO/Kaolin Nanocomposite. The oxidative degradation reaction of MB with NaOCl was performed with and without the prepared catalyst materials. The intensity of the peak at λ_{max} of 664 nm showed a slight decline after 20 min of reaction between MB and NaOCl without the addition of the nanocomposite catalyst material, as illustrated in Figure 3A. This shows that the degradation of MB dye by the NaOCl oxidant alone is insignificant compared to that by the NiO/kaolin nanocomposite. Nonetheless, the addition of the NiO catalyst without a support increased the rate of oxidative degradation, demonstrating the catalytic impact of NiO on the degradation of MB dye (Figure 3B). This was demonstrated by the MB's deep blue hue gradually decreasing and then disappearing, as well as the drop in λ_{max} intensity at 664 nm. The addition of the NiO/kaolin nanocomposite increases the catalytic activity very fast as the peak at λ_{max} of 664 nm fades quickly and becomes almost zero at 15 min, as shown in Figure 3C, indicating the complete degradation of the MB solution. Additionally, the removal capacity of kaolin alone and with NaOCl (Figure 3D,E, respectively) was evaluated. The results showed the peak decline of MBdye but it was not comparable with the composite. This is attributed to the adsorption capacity of kaolin toward methylene blue dye[37] and the small catalytic removal capacity of kaolin due to the presence of metal impurities like iron oxide and titanium oxide.[38]

3.2.3. Effect of Load Amount of NiO on Kaolin. The amount of NiO NPs on the kaolin surface could affect the catalytic process. To monitor the NiO loading amount on the substrate surface, the synthesis was completed with many trials of different mass compositions of $Ni(NO_3)_2{\cdot}6H_2O$ in a fixed amount of kaolin. The obtained materials among them were labeled as NiO/kaolin nanocomposite-1, NiO/kaolin nanocomposite-2, NiO/kaolin nanocomposite-3, and NiO/kaolin nanocomposite-4, and were evaluated with NaOCl as an oxidizing agent to determine the optimal composition for the catalytic oxidative degradation of MB dye.

To ascertain the degradation rate (k_{app}), the kinetics of MB dye degradation using the four catalysts produced was also examined (Table S-1). The rate of catalytic degradation of MB dye was fitted to pseudo-first-order reaction kinetics. Additionally, Table 1 shows strong correlation coefficient values on the plot of ln C_t/C_o vs reaction time, suggesting that pseudo-first-order kinetics could adequately characterize the events.

Table 1. Experimental Results for Oxidative Degradation of MB Dye (50 mg/L)

	pseudo-first order		pseudo-second order	
T (k)	k_{app1} (min^{-1})	R^2	k_{app2} ($M^{-1}{\cdot}min^{-1}$)	R^2
298	0.1113	0.9968	1.6665	0.8881
306	0.1813	0.9985	2.8451	0.8248
313	0.2215	0.9972	2.3395	0.7676
320	0.2664	0.9969	2.6830	0.8221

The results of the two equations, the calculated rate constants k_{app1} and k_{app2}, and the correlation coefficients R^2 show that the R^2 for the pseudo-first-order model is higher than that for the pseudo-second-order model and close to 1, indicating that the oxidative degradation process is better described by the pseudo-first-order model.

The UV–vis spectra displayed in Figure S-2 show the removal of MB dye by four nanomaterials prepared in addition to the unmodified kaolin (Figure S-2A), indicating that the degradation of MB dye was significantly better with NiO/kaolin nanocomposite-2 (Figure S-2C) and NiO/kaolin nanocomposite-3 (Figure S-2D) than with NiO/kaolin nanocomposite-1 (Figure S-2B) and NiO/kaolin nanocomposite-4 (Figure S-2E). In the presence of NiO/kaolin nanocomposites-2 and –3, the peak at 664 nm nearly vanished within minutes. Additionally, for NiO/kaolin nanocomposites-1–3, the degradation rate constant, k_{app}, increased (0.14674, 0.2351, 0.25277 min^{-1}, respectively), and the highest removal efficiency for the oxidative degradation of MB dye was demonstrated by the lower rate with NiO/kaolin nanocomposite-4 (0.14057 min^{-1}; Figure 4). Under the same conditions, the degradation efficiency of NiO/kaolin nanocomposite-2 (10 mg) with NaOCl (4%) for 50 mL (50 mg L^{-1}) MB dye in a 15 min reaction time was 98.2%, whereas the NiO/kaolin composite-3

https://doi.org/10.1021/acsomega.3c05126
ACS Omega 2024, 9, 4287–4299

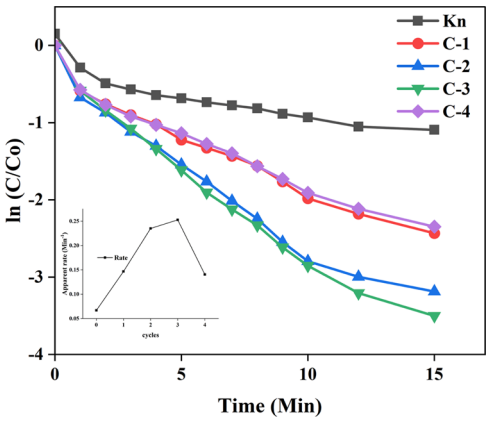

Figure 4. Pseudo-first-order plot of kaolin, C-1, C-2, C-3, and C-4. Conditions: 10 mg of catalyst; 50 mL (50 mg/L) of MB dye; 0.5 mL of NaOCl; 40 °C temperature.

had a removal efficiency of 98.5%. The k_{app} values for the NiO/kaolin nanocomposites-1−3 were 0.14674, 0.2351, and 0.25277 $min^{-1,}$ respectively. Therefore, choosing the best loading content of NiO is crucial. Since NiO/kaolin nanocomposite-2 showed an acceptable catalytic performance for MB dye degradation with a lower precursor mass, it was selected as the best catalyst for these experiments.

The mechanism of action is as follows: the support and metal oxide nanoparticles may perform as agents for the generation of free active oxidizing agents, yielding the extremely reactive oxidizing agent radicals (singlet oxygen ($^1O_2$)) that are able to degrade the organic molecules of the dye.[39,40]

The oxidative degradation at various temperatures was performed and fitted by using the pseudo-first- (eq 3) and -second-order reactions (eq 4) as follows[23]

$$\ln\frac{C_t}{C_o} = k_{app1}t \tag{3}$$

$$\frac{1}{C_t} = k_{app2}t + \frac{1}{C_o} \tag{4}$$

where C_o is the initial MB dye concentration (mg/L), C_t is the concentration of the residual MB dye (mg/L), t is the time (min), and k_{app1} and k_{app2} are the rate constants of the pseudo-first- (min^{-1}) and -second-order reactions ($M^{-1}\cdot min^{-1}$), respectively.

3.2.4. Impact of Operating Factors on the Catalytic Oxidative Activity of the NiO/Kaolin Nanocomposite. 3.2.4.1. Effect of Initial MB Dye Concentration. Three aqueous MB solutions with varying concentrations between 30 and 50 ppm were utilized in this work, along with a constant concentration of the catalyst (10 mg/50 mL) and NaOCl (4%, 0.5 mL). Figure S-3A−C shows the relevant UV−vis absorption spectra for the oxidative breakdown of MB at the necessary concentrations. As can be observed, the time needed for full degradation increased as the MB dye concentration increased. The degradation rate decreased as the MB dye concentration increased, thus supporting the first-order kinetics of the degradation process. This decline in the rate is caused by the electron transfer process between NaOCl and the MB dye slowing down on the nanocomposite surface, and excess MB competing with one another for the few active species made available by the kaolin−NiO process.[41] Figure 5 displays the pseudo-first-order kinetic graphs for different concentrations of MB dye.

3.2.4.2. Effect of Catalyst Dosage. We conducted four reactions by varying the quantity of NiO/kaolin nanocomposites from 5.5 to 20.1 mg (Figure S-4A−D) while maintaining the other reaction parameters constant to examine the impact of catalyst loading on the oxidative degradation of MB dye. Figure 6 displays the degradation trends of the aqueous MB dye (50 mL, 50 ppm) solution across the various nanocomposite quantities in addition to NaOCl (4%, 0.5 mL). As the loading of the nanocatalyst increased from 5.5 to 20.1 mg, it was observed that the degradation efficiency improved. In order to investigate other reaction parameters, a catalyst dosage of 10 mg was used. Due to the greater catalyst dosage, there were more active sites on the catalyst surface, which improved the catalyst's adsorption capacity and accelerated the rate at which NaOCl broke down.[42]

3.2.4.3. Effect of Temperature. We conducted four reactions, altering the temperature from room temperature to 47 °C, while maintaining the other reaction parameters

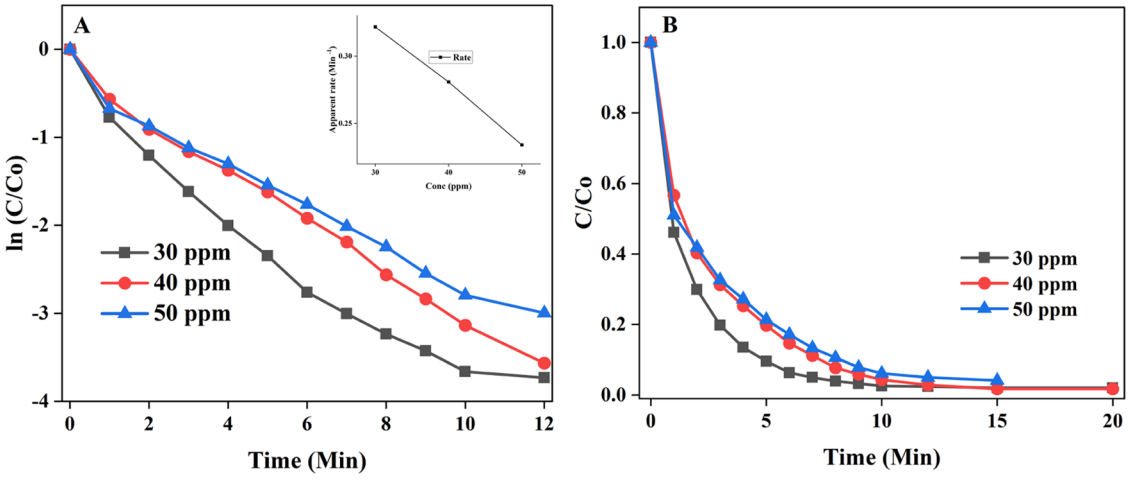

Figure 5. ln(C/C_o) vs time plot (a) and C/C_o vs time plot (b) of 50 mL of 30 ppm and 40 ppm MB and 50 ppm MB dye (conditions: 0.5 mL of 4% NaOCl and 10 mg of the nanocomposite).

https://doi.org/10.1021/acsomega.3c05126
ACS Omega 2024, 9, 4287−4299

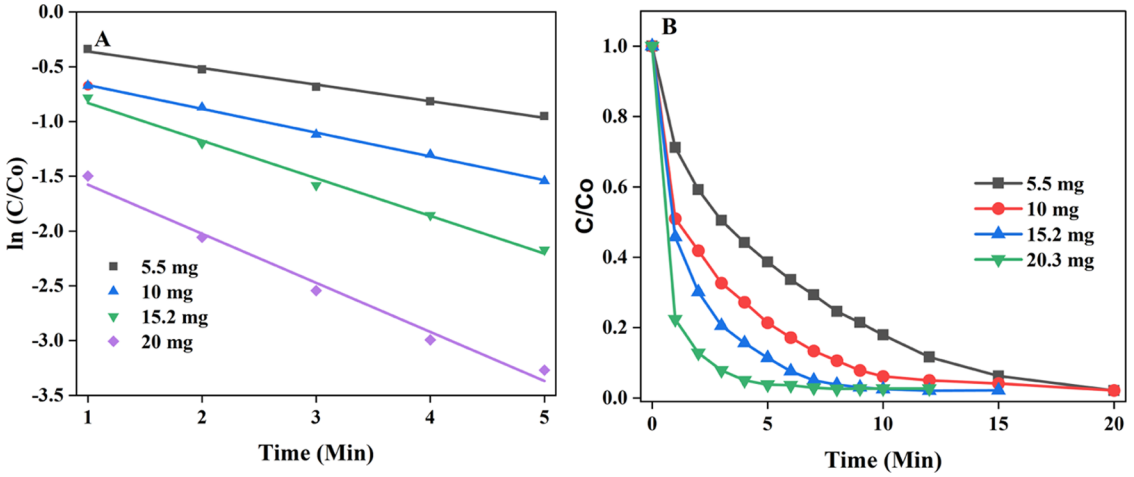

Figure 6. ln (C/C_o) vs time plot (A) and C/C_o vs time plot (B) of aqueous MB dye (50 mL,50 ppm) and 5.5, 10, 15.2, and 20 mg of the NiO/kaolin nanocomposite (conditions: 0.5 mL of 4% NaOCl and 40 °C temperature).

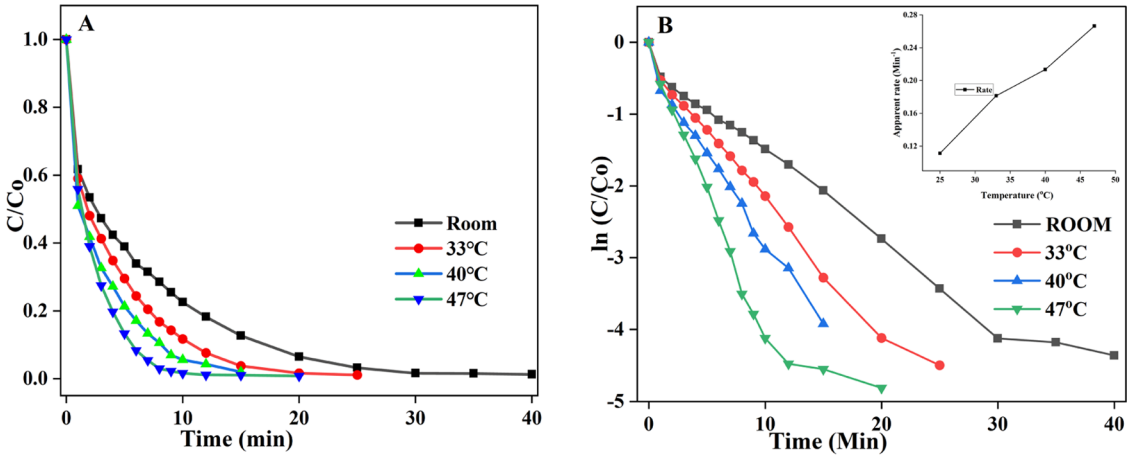

Figure 7. Degradation of MB dye at different temperatures: room temperature, 33, 40, and 47 °C. (A) C/C_o vs time and (B) ln(C/C_o) vs time plot.

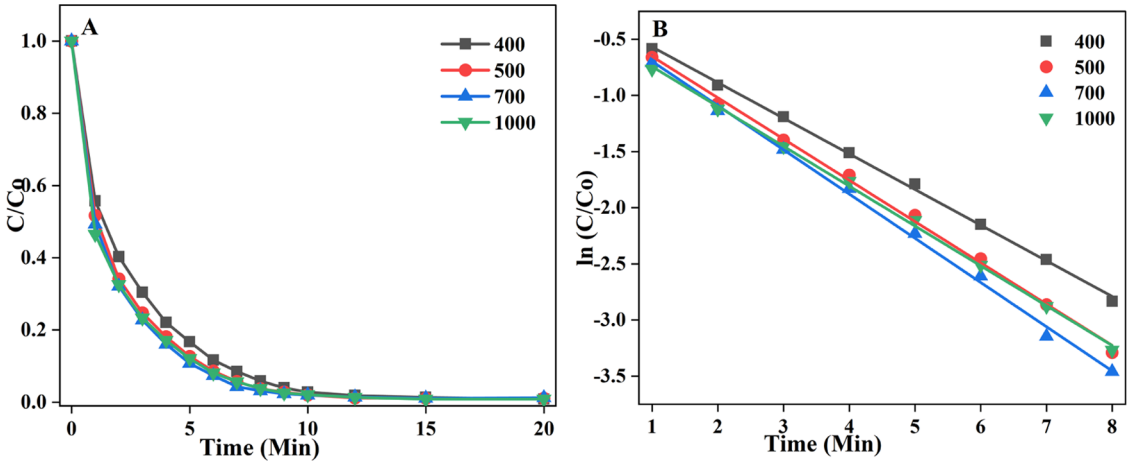

Figure 8. Degradation of 50 mL of 50 ppm MB with different NaOCl amounts (400, 500, 700, and 100 μL): (A) C/C_o vs time plot and (B) ln (C/C_o) vs time plot.

constant, to examine the impact of temperature on the oxidative degradation of MB dye. Figure S-5A–D displays the degradation curves of aqueous MB dye (50 ppm) solution at several temperatures, ranging from ambient temperature to 47 °C, in conjunction with NaOCl (4%, 0.5 mL) solution. Figure 7A (C/C_o) and B $(\ln(C/C_o))$ with time plot illustrates how the efficacy of oxidative degradation increases with temperature, from room temperature to 47 °C. According to these findings, the reaction's duration to reach equilibrium following heating might be considerably reduced by an increase in temperature. The breakdown efficiency of NaOCl might be improved by raising the temperature and increasing the rate of effective

https://doi.org/10.1021/acsomega.3c05126
ACS Omega 2024, 9, 4287−4299

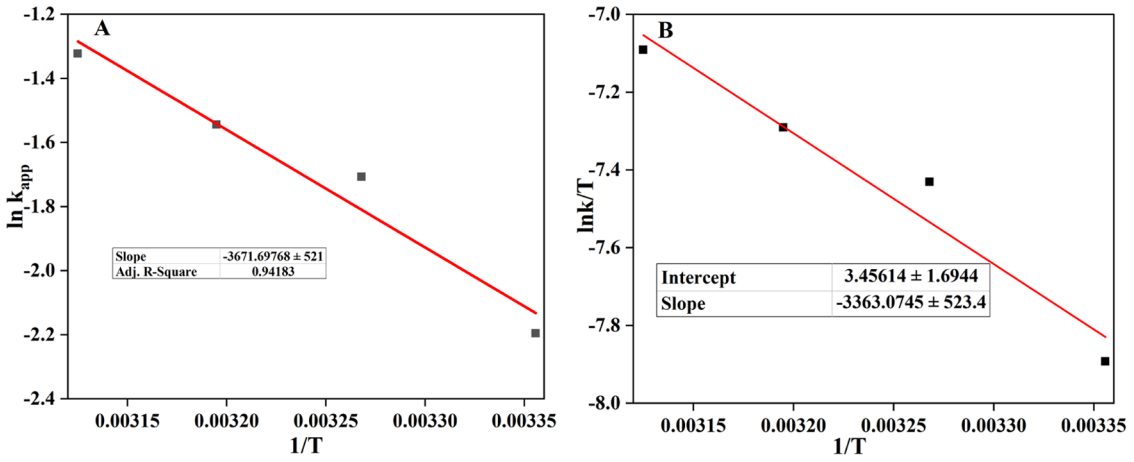

Figure 9. (a) $\ln k_{app}$ vs $1/T$ and (b) $\ln (k_{app}/T)$ vs $1/T$ plots for the oxidative degradation of 50 ppm of 50 mL MB dye.

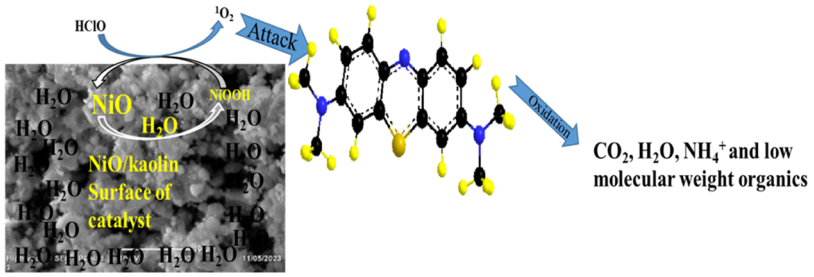

Figure 10. Proposed reaction mechanism for the degradation of MB dye by the NiO/Kn/NaOCl system.

collisions among the catalyst, MB, and other molecules. In the NiO/kaolin/NaOCl system, elevating the temperature might potentially accelerate the diffusion of MB dye onto the catalytic surface, eliminate intermediates from degradation, and re-expose the active sites by improving the mass transfer efficiency at the solid−liquid interface.[43] Hypochlorite can also form reactive oxygen species (ROS) when exposed to heat or UV light, and these ROS can further degrade, hydrolyze, or halogenate the pre-existing organic compounds.[44]

3.2.4.4. Effect of Hypochlorite Amount. We conducted many reactions, adjusting the quantity of hypochlorite in each reaction to examine the impact of NaOCl on the removal of MB dye. The best degradation was observed with volumes from 300 to 1000 μL by observing their UV−vis spectra (Figure S-6A−D). The degradation profiles of the aqueous MB dye (50 mL, 50 ppm) solution over different NaOCl concentrations and with 10 mg of the catalyst at 40 °C are shown in Figure 8, and it was found that the NaOCl amount had no major effect on catalysis once saturation was attained. Therefore, 500 μL was chosen for the experiments.

3.3. Thermodynamics and Kinetic Study of Oxidative Degradation of MB. To calculate the activation energy (E_a) and other thermodynamic parameters, the variations of k_{app} with temperature (298, 306, 313, 320 K) were utilized. The Arrhenius equation was used to determine the catalytic degradation's activation energy.[45]

$$\ln k_{app} = -\frac{E_a}{RT} + \ln A \tag{5}$$

Here, A is the Arrhenius constant (min^{-1}), E_a is the energy of activation (kJ/mol), k_{app} is the apparent rate constant (min^{-1}), T is the temperature (k), and R is the universal gas constant (=8.314; J/mol K). To calculate the activation energy, we plotted $\ln(k)$ vs $1/T$ and obtained a straight line, and the activation energy was calculated from its slope. The data obtained from the degradation experiments at 298, 306, 313, and 320 K are shown in Figure 9 The flowing Eyring equation was used to calculate the thermodynamic parameters using the initial MB dye concentrations of 50 mg/L.[46]

$$\ln\frac{k_{app}}{T} = -\frac{\Delta H^*}{RT} + \ln\frac{k_B}{h} + \frac{\Delta S^*}{R} \tag{6}$$

Here, k_{app} is the rate constant, T is the temperature, ΔH^* is the enthalpy, ΔS^* is the entropy, K_B is the Boltzmann constant (=1.3 × 10^{-23} m^2 kg s^{-2} K^{-1}), h is the Plancks constant (=6.626 × 10^{-34} m^2 kgs^{-1}), and R is the universal gas constant (=8.314 J mol^{-1} K^{-1}).

We have a straight line, and we can obtain the enthalpy and entropy, respectively, from its slope and intercept.[47]

ΔG^* can also be calculated by the following equation

$$\Delta G^* = \Delta H^* - T\Delta S^* \tag{7}$$

The activation energy value with NiO/kaolin/NaOCl was found to be 30.5 kJ/mol, showing that the catalysis proceeds with less activation energy. A negative ΔS^* indicates instability of the system where degradation took place. The positive ΔH^* value denotes an endothermic reaction, and the free energy increases as temperature increases, indicating that the spontaneity of a catalysis system increases as shown in Table S-2.[48] The overall summary of the effect of operational parameters is given in Table S-3

3.4. Proposed Mechanism and the Possible Pathway for the Degradation of MB Dye with the NiO/Kaolin/NaOCl System. The degradation mechanism of MB dye by the NiO/kaolin/NaOCl system is proposed in Figure 10, and it is supposed that the support and metal oxide nanoparticles

https://doi.org/10.1021/acsomega.3c05126
ACS Omega 2024, 9, 4287−4299

Table 2. Comparison of the Removal Activity of the NiO/kaolin Nanocomposite for the Degradation of MB Dye with Catalysts Reported in the Literature

catalyst	catalyst dosage	MB dye conc (mg/L)	oxidizing agent	time (min)	temperature (°C)	removal percentage (%)	refs
Ni−Fe/Al_2O_3	20 mg/mL	50	NaOCl	40	45	98.98	39
CFACoFe_2O_4	12 gm/100 mL	40	5 mM H_2O_2	60	room	99	51
PANI-Ag/ZnS	30 mg/L	10	3 mM H_2O_2	60	room	>95	52
CoO	0.5 mg/mL	12	NaOCl	25		>96	53
Cu_2O−Cu/C	0.2 mg/mL		0.03 M H_2O_2	40	50	>99	54
CuO	10 mg/50 mL	10	12% NaOCl	30	32	95	55
NiO/kaolin	20.3 mg/50 mL	50	4% NaOCl	6	40	>99	this work

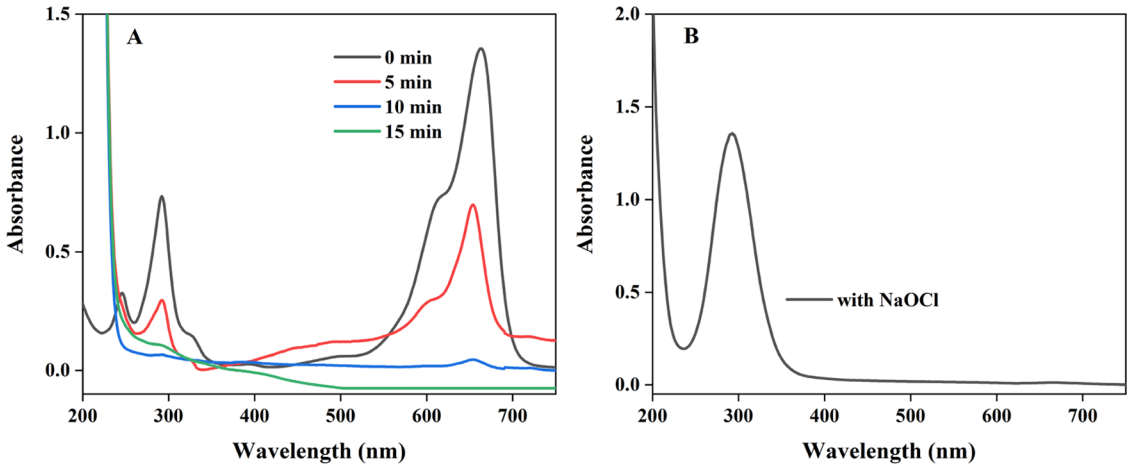

Figure 11. UV−vis spectra for the degradation of MB dye with the NiO/kaolin/NaOCl system: (A) NaOCl removed the degradation products and (B) degradation product after 15 min with NaOCl (conditions: 10 mg of NiO/kaolin; 50 mL of 50 ppm MB; 40 °C; 0.5 mL of 4%NaOCl).

act as agents for the generation of free active oxidizing agents, yielding the extremely reactive oxidizing agent radicals (singlet oxygen ($^1O_2$)) that are able to degrade the organic molecules of the dye. The possible intermediates in the degradation of MB with the NaOCl system are available in the literature,[39] and they indicate that the main steps of MB dye degradation are demethylation, chromophore cleavage, ring opening, and mineralization.[39,49]

The oxidative degradation reaction of MB dye leads to the creation of CO_2 and the transformation of heteroatoms of nitrogen and sulfur to inorganic ions, such as ammonium, nitrate, and sulfate ions, and the catalyst that we synthesized showed supreme catalytic activity when it was compared with some literature studies (Table 2).[40,50]

Step one (I)

$$NaClO + H_2O \rightarrow HOCl + NaOH \quad (8)$$

$$HOCl + MB \rightarrow CO_2 + H_2O + \text{by product} \quad (9)$$

Step two (II)

$$2NiO + OCl^- + H_2O \rightarrow 2NiOOH + {}^1O_2 + Cl^- \quad (10)$$

$$NiOOH + H_2O \rightarrow NiO + O_2 + 3H^+ \quad (11)$$

$$({}^1O_2 + MB \rightarrow CO_2 + H_2O + \text{by product} \quad (12)$$

3.5. Quenching Experiments. *3.5.1. Degradation Confirmation Test.* In this work, 5 mL of methylene blue and hypochlorite-containing water was centrifuged to remove the solid catalyst, and 10 mL of DCM was added to this solution and shaken for 2 min. The MB dye residue, transferred from water to DCM, and NaOCl remain in the aqueous phase as they are easily soluble in water.[57] The final product was pipetted out and transferred to a cuvette to obtain the final result. The UV−vis spectra of the extracted solution obtained at different times were measured, and the complete degradation of the methylene blue dye was observed after 15 min, as shown in Figure 11A.

Finally, in order to check the complete removal of the MB dye, the separation of hypochlorite from the methylene blue dye solution was performed because hypochlorite has a large absorbance peak at 293 nm, which can mask the MB dye peak at a wavelength of 290 nm, as shown in Figure 11B. Therefore, extraction was necessary to determine the degradation pattern of MB dye. Thus, by employing dichloromethane (DCM) as an extractant, the extraction of MB dye from aqueous solutions has been investigated. Dichloroethane, xylene, toluene, and benzene are among several extractants utilized in the literature. It was determined that dichloromethane was the most effective active extractant for extracting the MB dye.[56]

3.5.2. Reusability of the Nanocomposite. The material's capacity for reuse and the metal ion discharge analysis are crucial markers for assessing the material's stability.[58] Although the NiO/kaolin nanocomposite offers great catalytic performance, it is vital to investigate its recycling stability. Therefore, NiO/kaolin was isolated and reused for degrading MB dye to determine its effectiveness upon recycling. As shown in Figure 12, the catalytic performance of NiO/kaolin was not reduced considerably after six cycles for the degradation of MB dye, which indicates the high stability of NiO/kaolin. The conversion percentage of the MB dye decreased slightly after the catalyst was recycled six times, probably due to mass loss, the decrease of active sites by NiO escape, and the partly adsorption-covered active sites on the catalyst surface.[59]

https://doi.org/10.1021/acsomega.3c05126
ACS Omega 2024, 9, 4287−4299

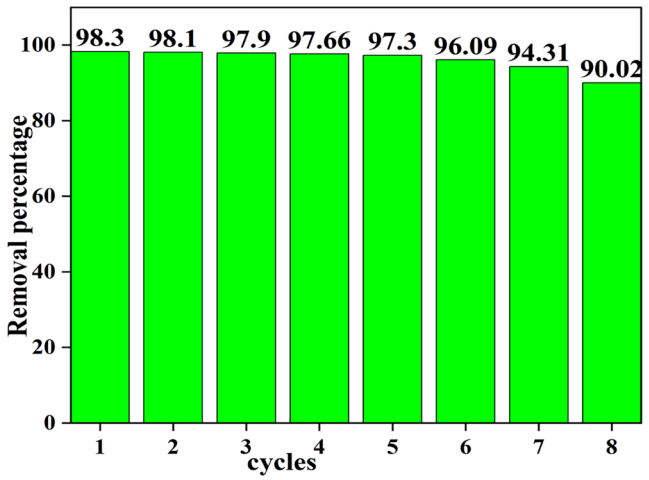

Figure 12. Recyclability of the NiO/kaolin nanocomposite; removal efficiency (green).

XRD data were obtained for the material used 8 times (Figure S-7). It was observed that the 200 diffraction plane of the NiO catalyst is comparatively reduced in intensity relative to that of the 111 plane, signifying that the active surface of the catalyst was 200 and reduced as a result of its catalytic activity. This is in agreement with the decreased percentage removal efficiency (90.02% at the eighth cycle) of the NiO catalyst.

4. CONCLUSIONS

In summary, we have proved that a highly efficient NiO/kaolin nanocomposite and NiO alone can be successfully synthesized and applied to remove methylene blue from aqueous solutions in the presence of NaOCl by facilitating the decomposition of NaOCl. A simple and cost-effective wet impregnation and co-precipitation method was employed for the synthesis of NiO/kaolin and NiO alone, respectively. The kaolin employed in this investigation served as the substrate and support for the nanoscale NiO particles. The synthesized nanocomposite was characterized using UV−vis, FT-IR, SEM, and XRD, and it was found to be well distributed on the surface of kaolin without aggregation. From UV−vis spectroscopic data, characteristic peaks were observed at a wavelength of 333 nm, which confirms the formation of NiO NPs on the surface of kaolin. The crystal sizes of NiO and NiO/kaolin obtained from XRD were 11 and 3 nm, respectively. The synthesized NiO/kaolin nanocomposite was employed as a catalyst toward the oxidative degradation of MB dye and showed high catalytic activity. The oxidation proceeded according to pseudo-first-order kinetics with temperature, dye concentration, and nanocatalyst load, all of which had a significant impact on the reaction rate. The ideal loading quantity of NiO NPs on the kaolin surface was responsible for its exceptional catalytic degradation properties. In the presence of 0.5 mL of 4% NaOCl, the NiO/kaolin combination (20.3 mg) broke down 99% of 50 mL of 50 mg/L MB dye solution in 6 min at a rate of 0.4462 min^{-1}. In addition, the NiO/kaolin nanocomposite exhibited outstanding catalytic activity, stability, and strong reusability, suggesting that it may be a viable option for treating wastewater discharged from industries.

ASSOCIATED CONTENT

Supporting Information

The Supporting Information is available free of charge at https://pubs.acs.org/doi/10.1021/acsomega.3c05126.

XRD spectra of kaolin−NiO nanocomposites (Figure S-1); UV−vis spectra of the degradation of MB with bare kaolin and different compositions of kaolin and NiO (Figure S-2); kinetic parameters of four different catalysts with the same conditions as NaOCl (Table S-1); UV−vis spectra of the effect of initial MB dye concentration, catalyst dosage, the effect of temperature, and the effect of hypochlorite amount on the degradation efficiency of the catalyst (Figure S3−S6); thermodynamic and kinetic parameters of one of the best catalysts selected (Table S-2); summary of different reaction parameters (Table S-3), XRD spectra of the kaolin−NiO nanocomposite after eight cycles of catalysis (Figure S-7) (PDF)

AUTHOR INFORMATION

Corresponding Authors

Minaleshewa Atlabachew − *Department of Chemistry, College of Science, Bahir Dar University, Bahir Dar 6000, Ethiopia;* orcid.org/0000-0003-3261-8326; Email: atminale2004@yahoo.com

Belete Asefa Aragaw − *Department of Chemistry, College of Science, Bahir Dar University, Bahir Dar 6000, Ethiopia;* orcid.org/0000-0003-4801-7197; Email: beliyeeed@gmail.com

Authors

Kedir Seid Mohammed − *Department of Chemistry, College of Science, Bahir Dar University, Bahir Dar 6000, Ethiopia;* Present Address: Department of Chemistry, College of Science, Wollo University, Wollo, Ethiopia

Zinabu Gashaw Asmare − *Department of Chemistry, College of Science, Bahir Dar University, Bahir Dar 6000, Ethiopia;* Present Address: Department of Chemistry, College of Natural and Computational Sciences, Debre Tabor University, P.O. Box 272, Debre Tabor, Ethiopia.; orcid.org/0000-0002-8945-6172

Complete contact information is available at: https://pubs.acs.org/10.1021/acsomega.3c05126

Notes

The authors declare no competing financial interest.

ACKNOWLEDGMENTS

We thank Wollo University for supporting Kedir Seid Mohammed during his M.Sc. The authors express their gratitude to the Science College at Bahir Dar University for providing laboratory space and related amenities. The College of Science at Bahir Dar University provided funding for this work in part under the Mega Project (Mega Project-2020).

REFERENCES

(1) Jadoun, S.; Fuentes, J. P.; Urbano, B. F.; Yáñez, J. A review on adsorption of heavy metals from wastewater using conducting polymer-based materials. *J. Environ. Chem. Eng.* **2023**, *11* (1), No. 109226.

(2) Tang, L. L.; DeNardo, M. A.; Schuler, C. J.; Mills, M. R.; Gayathri, C.; Gil, R. R.; Kanda, R.; Collins, T. J. Homogeneous

catalysis under ultradilute conditions: TAML/NaClO oxidation of persistent metaldehyde. *J. Am. Chem. Soc.* **2017**, *139* (2), 879−887.
(3) Doan, V.-D.; Nguyen, N.-V.; Nguyen, T. L.-H.; Tran, V. A.; Le, V. T. High-efficient reduction of methylene blue and 4-nitrophenol by silver nanoparticles embedded in magnetic graphene oxide. *Environ. Sci. Pollut. Res.* **2023**, *30*, 71543−71553.
(4) Xu, Z.; Zhang, Q.; Li, X.; Huang, X. A critical review on chemical analysis of heavy metal complexes in water/wastewater and the mechanism of treatment methods. *Chem. Eng. J.* **2022**, *429*, No. 131688.
(5) Zhang, T. J. A. O. P. Heterogeneous catalytic process for wastewater treatment. 2020, *17*.
(6) Cui, Y.; Ma, K.; Chen, Z.; Yang, J.; Geng, Z.; Zeng, J. Atomic-level insights into strain effect on p-nitrophenol reduction via Au@ Pd core−shell nanocubes as an ideal platform. *J. Catal.* **2020**, *381*, 427−433.
(7) Luneau, M.; Lim, J. S.; Patel, D. A.; Sykes, E. C. H.; Friend, C. M.; Sautet, P. Guidelines to achieving high selectivity for the hydrogenation of α, β-unsaturated aldehydes with bimetallic and dilute alloy catalysts: a review. *Chem. Rev.* **2020**, *120* (23), 12834−12872.
(8) Begum, R.; Najeeb, J.; Sattar, A.; Naseem, K.; Irfan, A.; Al-Sehemi, A. G.; Farooqi, Z. H. Chemical reduction of methylene blue in the presence of nanocatalysts: a critical review. *Rev. Chem. Eng.* **2020**, *36* (6), 749−770. Sherazi, T. H. Evaluation of Physico-chemical Properties in Selected Branded Soaps. *Pak. J. Anal. Environ. Chem.* **2019**, *20* (2), 177−183.
(9) Ghoniem, M. G.; Ali, F. A. M.; Abdulkhair, B. Y.; Elamin, M. R. A.; Alqahtani, A. M.; Rahali, S.; Ben Aissa, M. A. Highly selective removal of cationic dyes from wastewater by MgO nanorods. *Nanomaterials* **2022**, *12* (6), 1023. Shuang, S.; Zhang, Z. The effect of annealing treatment and atom layer deposition to Au/Pt nanoparticles-decorated TiO2 nanorods as photocatalysts. *Molecules* **2018**, *23* (3), 525.
(10) Rezvani, M. A.; Miri, O. F. Synthesis and characterization of PWMn/NiO/PAN nanosphere composite with superior catalytic activity for oxidative desulfurization of real fuel. *Chem. Eng. J.* **2019**, *369*, 775−783.
(11) Ifijen, I. H.; Maliki, M.; Anegbe, B. Synthesis, photocatalytic degradation and antibacterial properties of selenium or silver doped zinc oxide nanoparticles: A detailed review. *OpenNano* **2022**, *8*, No. 100082.
(12) Rahman, Q. I.; Ahmad, M.; Misra, S. K.; Lohani, M. Effective photocatalytic degradation of rhodamine B dye by ZnO nanoparticles. *Mater. Lett.* **2013**, *91*, 170−174.
(13) Wu, Y.; Kong, L. Advance on toxicity of metal nickel nanoparticles. *Environ. Geochem. Health* **2020**, *42*, 2277−2286.
(14) Sirelkhatim, A.; Mahmud, S.; Seeni, A.; Kaus, N. H. M.; Ann, L. C.; Bakhori, S. K. M.; Hasan, H.; Mohamad, D. Review on zinc oxide nanoparticles: antibacterial activity and toxicity mechanism. *Nano-Micro Lett.* **2015**, *7*, 219−242.
(15) Zou, Y.; Hu, Y.; Shen, Z.; Yao, L.; Tang, D.; Zhang, S.; Wang, S.; Hu, B.; Zhao, G.; Wang, X. Application of aluminosilicate clay mineral-based composites in photocatalysis. *J. Environ. Sci.* **2022**, *115*, 190−214. Padil, V. V. T.; Kumar, K. A.; Murugesan, S.; Torres-Mendieta, R.; Wacławek, S.; Cheong, J. Y.; Černík, M.; Varma, R. S. Sustainable and safer nanoclay composites for multifaceted applications. *Green Chem.* **2022**, *24* (8), 3081−3114. Mundkur, N.; Khan, A. S.; Khamis, M. I.; Ibrahim, T. H.; Nancarrow, P. Synthesis and characterization of clay-based adsorbents modified with alginate, surfactants, and nanoparticles for methylene blue removal. *Environ. Nanotechnol., Monit. Manage.* **2022**, *17*, No. 100644.
(16) Zyoud, A. H.; Zubi, A.; Zyoud, S. H.; Hilal, M. H.; Zyoud, S.; Qamhieh, N.; Hajamohideen, A.; Hilal, H. Kaolin-supported ZnO nanoparticle catalysts in self-sensitized tetracycline photodegradation: zero-point charge and pH effects. *Appl. Clay Sci.* **2019**, *182*, No. 105294.
(17) Mundkur, N.; Khan, A. S.; Khamis, M. I.; Ibrahim, T. H.; Nancarrow, P. Synthesis and characterization of clay-based adsorbents modified with alginate, surfactants, and nanoparticles for methylene blue removal. *Environ. Nanotechnol., Monit. Manage.* **2022**, *17*, No. 100644.
(18) Asghar, A.; Raman, A. A. A.; Daud, W. M. A. W. In situ production of hydrogen peroxide in a microbial fuel cell for recalcitrant wastewater treatment. *J. Chem. Technol. Biotechnol.* **2017**, *92* (7), 1825−1840.
(19) Teixeira, L. A. C.; Arellano, M. T. C.; Sarmiento, C. M.; Yokoyama, L.; da Fonseca Araujo, F. V. Oxidation of cyanide in water by singlet oxygen generated by the reaction between hydrogen peroxide and hypochlorite. *Miner. Eng.* **2013**, *50*−*51*, 57−63.
(20) Behin, J.; Akbari, A.; Mahmoudi, M.; Khajeh, M. Sodium hypochlorite as an alternative to hydrogen peroxide in Fenton process for industrial scale. *Water Res.* **2017**, *121*, 120−128.
(21) Han, X.; Wang, Z.; Wang, X.; Zheng, X.; Ma, J.; Wu, Z. Microbial responses to membrane cleaning using sodium hypochlorite in membrane bioreactors: Cell integrity, key enzymes and intracellular reactive oxygen species. *Water Res.* **2016**, *88*, 293−300.
(22) Huang, W.-C.; Kim, J.-D. Nickel oxide nanoparticle-based method for simultaneous harvesting and disruption of microalgal cells. *Bioresour. Technol.* **2016**, *218*, 1290−1293.
(23) Aragaw, T. A.; Angerasa, F. T. J. H. Synthesis and characterization of Ethiopian kaolin for the removal of basic yellow (BY 28) dye from aqueous solution as a potential adsorbent. *Heliyon* **2020**, *6* (9), No. e04975.
(24) Asmare, Z. G.; Aragaw, B. A.; Atlabachew, M.; Wubieneh, T. A. Kaolin-Supported Silver Nanoparticles as an Effective Catalyst for the Removal of Methylene Blue Dye from Aqueous Solutions. *ACS Omega* **2023**, *8* (1), 480−491.
(25) Zhang, Y.-X.; Tang, S.; Zhang, W.-D.; Yu, Y.-X. Noble Metal-Free Photocatalysts Consisting of Graphitic Carbon Nitride, Nickel Complex, and Nickel Oxide Nanoparticles for Efficient Hydrogen Generation. *ACS Appl. Mater. Interfaces* **2019**, *11* (16), 14986−14996.
(26) Moumen, A.; Belhocine, Y.; Sbei, N.; Rahali, S.; Ali, F. A. M.; Mechati, F.; Hamdaoui, F.; Seydou, M. Removal of Malachite Green Dye from Aqueous Solution by Catalytic Wet Oxidation Technique Using Ni/Kaolin as Catalyst. *Molecules* **2022**, *27* (21), 7528.
(27) Noginov, M. A.; Zhu, G.; Bahoura, M.; Adegoke, J.; Small, C.; Ritzo, B.; Drachev, V.; Shalaev, V. M. Enhancement of surface plasmons in an Ag aggregate by optical gain in a dielectric medium. *Opt. Lett.* **2006**, *31* (20), 3022−3024.
(28) Iqbal, J.; Abbasi, B. A.; Ahmad, R.; Mahmoodi, M.; Munir, A.; Zahra, S. A.; Shahbaz, A.; Shaukat, M.; Kanwal, S.; Uddin, S.; et al. Phytogenic synthesis of nickel oxide nanoparticles (NiO) using fresh leaves extract of Rhamnus triquetra (wall.) and investigation of its multiple in vitro biological potentials. *Biomedicines* **2020**, *8* (5), 117. Haider, A.; Ijaz, M.; Ali, S.; Haider, J.; Imran, M.; Majeed, H.; Shahzadi, I.; Ali, M. M.; Khan, J. A.; Ikram, M. Green synthesized phytochemically (Zingiber officinale and Allium sativum) reduced nickel oxide nanoparticles confirmed bactericidal and catalytic potential. *Nanoscale Res. Lett.* **2020**, *15*, No. 50.
(29) Kganyago, P.; Mahlaule-Glory, L.; Mathipa, M.; Ntsendwana, B.; Mketo, N.; Mbita, Z.; Hintsho-Mbita. Synthesis of NiO nanoparticles via a green route using Monsonia burkeana: the physical and biological properties. *J. Photochem. Photobiol., B* **2018**, *182*, 18−26.
(30) Diallo, A.; Kaviyarasu, K.; Ndiaye, S.; Mothudi, B.; Ishaq, A.; Rajendran, V.; Maaza, M. Structural, optical and photocatalytic applications of biosynthesized NiO nanocrystals. *Green Chem. Lett. Rev.* **2018**, *11* (2), 166−175. Srihasam, S.; Thyagarajan, K.; Korivi, M.; Lebaka, V. R.; Mallem, S. P. R. Phytogenic generation of NiO nanoparticles using Stevia leaf extract and evaluation of their in-vitro antioxidant and antimicrobial properties. *Biomolecules* **2020**, *10* (1), 89.
(31) Moavi, J.; Buazar, F.; Sayahi, M. H. Algal magnetic nickel oxide nanocatalyst in accelerated synthesis of pyridopyrimidine derivatives. *Sci. Rep.* **2021**, *11* (1), No. 6296.
(32) Aimdate, K.; Srifa, A.; Koo-Amornpattana, W.; Sakdaronnarong, C.; Klysubun, W.; Kiatphuengporn, S.;

https://doi.org/10.1021/acsomega.3c05126
ACS Omega 2024, 9, 4287−4299

Assabumrungrat, S.; Wongsakulphasatch, S.; Kaveevivitchai, W.; Sudoh, M. J. A. o.; et al. Natural kaolin-based Ni catalysts for CO2 methanation: On the effect of ce enhancement and microwave-assisted hydrothermal synthesis. *ACS Omega* **2021**, *6* (21), 13779−13794.
(33) Aragaw, T. A.; Angerasa, F. T. Synthesis and characterization of Ethiopian kaolin for the removal of basic yellow (BY 28) dye from aqueous solution as a potential adsorbent. *Heliyon* **2020**, *6* (9), No. e04975.
(34) Tahir, H.; Atika, S.; Muhammad, S. Synthesis of kaolin loaded Ag and Ni nanocomposites and their applicability for the removal of malachite green oxalate dye. *Iran. J. Chem. Chem. Eng.* **2018**, *37* (3), 11−22.
(35) Xue, H.; Dong, X.; Fan, Y.; Ma, X.; Yao, S. Study of Structural Transformation and Chemical Reactivity of Kaolinite-Based High Ash Slime during Calcination. *Miner. Eng.* **2023**, *13* (4), No. 466.
(36) Skiba, M.; Vorobyova, V. Green synthesis and characterization of silver nanoparticles using Prunus persica L.(peach pomace) with natural deep eutectic solvent and plasma-liquid process. *Chem. Pap.* **2022**, *76* (9), 5789−5806.
(37) Harrou, A.; Gharibi, E.; Nasri, H.; El Ouahabi, M. Thermodynamics and kinetics of the removal of methylene blue from aqueous solution by raw kaolin. *SN Appl. Sci.* **2020**, *2* (2), No. 277.
(38) Biswas, B.; Islam, M. R.; Deb, A. K.; Greenaway, A.; Warr, L. N.; Naidu, R. Understanding Iron Impurities in Australian Kaolin and Their Effect on Acid and Heat Activation Processes of Clay. *ACS Omega* **2023**, *8* (6), 5533−5544.
(39) Guo, X.; Chen, S.; Liu, Z.; Yang, C.; Chen, W. Catalytic oxidation of methylene blue by using Ni-Fe bimetallic catalyst/NaClO system: Performance, kinetics, mechanism, and DFT calculations. *Sep. Purif. Technol.* **2023**, *306*, No. 122612.
(40) Wu, K.; Shi, M.; Pan, X.; Zhang, J.; Zhang, X.; Shen, T.; Tian, Y. Decolourization and biodegradation of methylene blue dye by a ligninolytic enzyme-producing Bacillus thuringiensis: degradation products and pathway. *Enzyme Microb. Technol.* **2022**, *156*, No. 109999.
(41) Li, X.; Qin, Y.; Jia, Y.; Wang, R.; Ye, Z.; Zhou, M. Persulfate activation by novel iron−carbon composites for organic contaminant removal: Performance, mechanism, and DFT calculations. *Sep. Purif. Technol.* **2022**, *281*, 119962. Hong, P.; Wu, Z.; Yang, D.; Zhang, K.; He, J.; Li, Y.; Xie, C.; Yang, W.; Yang, Y.; Kong, L.; Liu, J. Efficient generation of singlet oxygen (1O2) by hollow amorphous Co/C composites for selective degradation of oxytetracycline via Fenton-like process. *Chem. Eng. J.* **2021**, *421*, No. 129594.
(42) Ding, H.; Hu, J. Degradation of carbamazepine by UVA/WO3/hypochlorite process: Kinetic modelling, water matrix effects, and density functional theory calculations. *Environ. Res.* **2021**, *201*, No. 111569. Yin, R.; Guo, W.; Wang, H.; Du, J.; Wu, Q.; Chang, J.-S.; Ren, N. Singlet oxygen-dominated peroxydisulfate activation by sludge-derived biochar for sulfamethoxazole degradation through a nonradical oxidation pathway: Performance and mechanism. *Chem. Eng. J.* **2019**, *357*, 589−599.
(43) Di, J.; Jamakanga, R.; Chen, Q.; Li, J.; Gai, X.; Li, Y.; Yang, R.; Ma, Q. Degradation of Rhodamine B by activation of peroxymonosulfate using Co3O4-rice husk ash composites. *Sci. Total Environ.* **2021**, *784*, No. 147258. Sun, Y.; Yang, Z.; Tian, P.; Sheng, Y.; Xu, J.; Han, Y.-F. Oxidative degradation of nitrobenzene by a Fenton-like reaction with Fe-Cu bimetallic catalysts. *Appl. Catal., B* **2019**, *244*, 1−10.
(44) Zou, X.; Li, X.; Chen, C.; Zhu, X.; Huang, X.; Wu, Y.; Pi, Z.; Chen, Z.; Tao, Z.; Wang, D.; Yang, Q. Degradation performance of carbamazepine by ferrous-activated sodium hypochlorite: Mechanism and impacts on the soil system. *Chem. Eng. J.* **2020**, *389*, 123451. Qin, L.; Lin, Y.-L.; Xu, B.; Hu, C.-Y.; Tian, F.-X.; Zhang, T.-Y.; Zhu, W.-Q.; Huang, H.; Gao, N.-Y. Kinetic models and pathways of ronidazole degradation by chlorination, UV irradiation and UV/chlorine processes. *Water Res.* **2014**, *65*, 271−281.
(45) Jensen, F. J. Q. Activation energies and the Arrhenius equation. *Qual. Reliab. Eng. Int.* **1985**, *1* (1), 13−17.
(46) Keusch, P. *Eyring Equation*; Citeseer, 2003.
(47) Raheb, I.; Manlla, M. S. Kinetic and thermodynamic studies of the degradation of methylene blue by photo-Fenton reaction. *Heliyon* **2021**, *7* (6), No. e07427.
(48) Abou-Gamra, Z. M. Kinetic and thermodynamic study for fenton-like oxidation of amaranth red dye. *Adv. Chem. Eng. Sci.* **2014**, *04*, No. 47576.
(49) Zhu, R.; Shen, Y.; Zhao, J.; Shi, G.; Liu, J.; Cao, J. Study on decolorization of methylene blue with a kind of electrolytic active water. *Text. Res. J.* **2023**, *93* (11−12), 2531−2544.
(50) Zhi, S.; Tian, L.; Li, N.; Zhang, K. A novel system of MnO2-mullite-cordierite composite particle with NaClO for Methylene blue decolorization. *J. Environ. Manage.* **2018**, *213*, 392−399.
(51) Nadeem, N.; Yaseen, M.; Rehan, Z. A.; Zahid, M.; Shakoor, R. A.; Jilani, A.; Iqbal, J.; Rasul, S.; Shahid, I. Coal fly ash supported CoFe2O4 nanocomposites: Synergetic Fenton-like and photocatalytic degradation of methylene blue. *Environ. Res.* **2022**, *206*, No. 112280.
(52) Mazhar, S.; Qazi, U. Y.; Nadeem, N.; Zahid, M.; Jalil, A.; Khan, F.; Ul-Hasan, I.; Shahid, I. Photocatalytic degradation of methylene blue using polyaniline-based silver-doped zinc sulfide (PANI-Ag/ZnS) composites. *Environ. Sci. Pollut. Res.* **2022**, *29* (6), 9203−9217.
(53) Stoyanova, M.; Christoskova, S. Catalytic degradation of methylene blue in aqueous solutions over Ni-and Co-oxide systems. *Open Chem.* **2011**, *9* (6), 1000−1007.
(54) Sun, B.; Li, H.; Li, X.; Liu, X.; Zhang, C.; Xu, H.; Zhao, X. Degradation of organic dyes over fenton-like Cu2O−Cu/C catalysts. *Ind. Eng. Chem. Res.* **2018**, *57* (42), 14011−14021.
(55) Farrouji, A.; Eddine, A. C.; Bouzit, S. E.; Boualy, B.; Mehdi, A.; El Firdoussi, L.; Ali, M. A. Degradation of methylene blue using synthesized nanostructured CuO with high specific surface area through catalytic oxidation. *Int. Res. J. Pure Appl. Chem.* **2015**, *8*, 190−197.
(56) El-Ashtoukhy, E. S. Z.; Fouad, Y. O. Liquid−liquid extraction of methylene blue dye from aqueous solutions using sodium dodecylbenzenesulfonate as an extractant. *Alexandria Eng. J.* **2015**, *54* (1), 77−81.
(57) Kirihara, M.; Okada, T.; Sugiyama, Y.; Akiyoshi, M.; Matsunaga, T.; Kimura, Y. Sodium Hypochlorite Pentahydrate Crystals (NaOCl·5H2O): A Convenient and Environmentally Benign Oxidant for Organic Synthesis. *Org. Process Res. Dev.* **2017**, *21* (12), 1925−1937.
(58) Wang, H.; Wang, H.; Yan, Q. Peroxymonosulfate activation by algal carbocatalyst for organic dye oxidation: Insights into experimental and theoretical. *Sci. Total Environ.* **2022**, *816*, No. 151611.
(59) Chen, Y.; Cui, K.; Cui, M.; Liu, T.; Chen, X.; Chen, Y.; Nie, X.; Xu, Z.; Li, C.-X. Insight into the degradation of tetracycline hydrochloride by non-radical-dominated peroxymonosulfate activation with hollow shell-core Co@NC: Role of cobalt species. *Sep. Purif. Technol.* **2022**, *289*, No. 120662.

https://doi.org/10.1021/acsomega.3c05126
ACS Omega 2024, 9, 4287−4299